N,*N*-Dialkylaniline-Substituted Tetraethynylethenes: A New Class of Chromophores Possessing an Emitting Charge-Transfer State. Experimental and Computational Studies.

Luca Gobbi,[b] Nuran Elmaci,[a] Hans Peter Lüthi,*[a] and François Diederich*[b]

The photophysical properties of N,N-dimethylaniline- (DMA) substituted tetraethynylethene (TEE; 3,4-diethynylhex-3-ene-1,5-diyne) and related derivatives were investigated in a joint experimental and computational study. Measurements of the electronic emission spectra showed that these novel chromophores display a dual fluorescence which strongly depends on solvent polarity. Computational studies suggest that the twisted intramolecular charge-transfer state (TICT) model offers a possible explanation for the experimentally observed dual fluorescence. Time-dependent density functional calculations revealed that the initial excited state reached upon photoirradiation relaxes to a lower-energy TICT state in which either the dimethylamino group is twisted into an orthogonal position with respect to the remaining planar arylated TEE moiety or the entire DMA donor group takes an orthogonal orientation with respect to the rigid, planar TEE acceptor moiety. For the compounds investigated, the charge-transfer state responsible for the strongly solvent-dependent luminescence is directly connected with the initial excited state, namely, no crossing of states is involved.
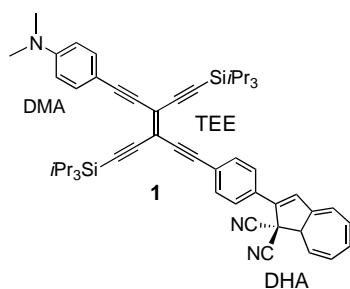
KEYWORDS:

alkynes · charge transfer · density functional calculations · fluorescence · TICT

Introduction

In the course of our investigations of the three-way chromophoric molecular switch **1**[1] (Scheme 1) featuring a TEE core[2] with DMA and arylated dihydroazulene (DHA) substituents, we remarked that the photochemical retroelectrocyclization of the DHA to the vinylheptafulvene (VHF) form[3] did take place only when the DMA moiety was protonated. In the absence of protonation, only slow but clean *trans – cis* isomerization of the central TEE core[4] was observed. These studies also demonstrated that compound **1**, with DMA as a strong donor and the DHA-appended TEE as a strong acceptor,[5, 6] undergoes efficient intramolecular donor – acceptor interactions. Accordingly, the UV/Vis spectrum of **1** features a bathochromically shifted charge-transfer band at $\lambda_{max} = 464$ nm. Upon protonation of the DMA group with trifluoroacetic acid, this band disappears and the longest-wavelength absorption maximum of $\mathbf{1} \cdot H^+$ shifts hypsochromically to $\lambda_{max} = 412$ nm, which is in the range of the maxima (404 – 420 nm) seen in the spectra of other TEE – DHA conjugates lacking the strong DMA donor.[1b]

Another remarkable feature of **1** is its emission behavior. Free **1** shows a strong fluorescence emission in solution that almost completely disappears after protonation with trifluoroacetic acid.[1, 7] In preliminary investigations, the maximum of this intense emission was found to be strongly dependent on solvent polarity, and in hexane a dual fluorescence ($\lambda_{max} = 505$ and 541 nm; $\lambda_{exc} = 420$ nm) was observed. In more polar solvents,

[a] Dr. H. P. Lüthi, Prof. N. Elmaci[+]
Laboratorium für Physikalische Chemie
Universitätsstrasse 16, ETH Zentrum
8092 Zürich (Switzerland)
Fax: (+41) 1-632-1615
E-mail: luethi@igc.phys.chem.ethz.ch

[b] Prof. F. Diederich, Dr. L. Gobbi
Laboratorium für Organische Chemie
Universitätsstrasse 16, ETH Zentrum
8092 Zürich (Switzerland)
Fax: (+41) 1-632-1109
E-mail: diederich@org.chem.ethz.ch

[+] Current address:
Department of Chemistry
İzmir Institute of Technology
Gülbahçe Köyü
İzmir 35437 (Turkey)

Scheme 1. The three-way chromophoric molecular switch **1** shows a dual fluorescence which is strongly solvent dependent.

such as CH_2Cl_2, the emission spectrum featured only a single, strongly red-shifted band ($\lambda_{max} = 602$ nm).

Dual fluorescence in organic donor – acceptor compounds was first reported by Lippert and co-workers in 1962.[8] The origin of the effect, however, is still somewhat controversial.[9, 10] There is general agreement on the fact that the first, higher-energy emission ("B-band") is due to the initial excitation to the locally excited (LE) state, and that the second, lower-energy band ("A-band") is due to emission from an internal charge-transfer (CT) state. The structure of the CT state, as well as the photochemical reaction coordinate connecting the two states, are the main sources of disagreement between the various models proposed.

The TICT model by Grabowski and co-workers[11, 12] assumes that the molecule from its LE state relaxes to a minimum on the excited-state surface by twisting the donor group into a plane perpendicular to the acceptor group. Along this twisting coordinate, there is an increase of the charge transfer from the donor to the acceptor group, which leads to the highly polar structure responsible for the A-band emission. Taking the example of 4-(*N,N*-dimethylanilino)benzonitrile (DMABN), the most intensely investigated compound in the context of dual fluorescence, the A-band would arise from a structure where the dimethylamino group is twisted by $\phi = 90°$ out of the plane of the benzonitrile moiety. In the planar intramolecular charge-transfer (PICT) model proposed by Zachariasse and co-workers,[13] on moving along the reaction coordinate from the LE to the CT state the molecule takes a strongly polar resonance structure (for DMABN: quinoid benzonitrile with a planar Me_2N group). The RICT model[14] of Sobolewski and Domcke, where R stands for rehybridized, assumes that the molecular structure of the CT state shows atomic rehybridization in the acceptor group as a result of the charge transfer (for DMABN: rehybridization of the cyano group carbon atom from sp to sp^2, planar Me_2N group, and quinoid benzene ring).

The present study was initiated to shed light on the photophysical behavior of the DMA – TEE donor – acceptor compound **1** in a combined experimental and computational approach. However, we anticipated that the relevance of experimental data would be reduced in view of the complexity of the system and the occurrence of competing *trans – cis* isomerization of the TEE core leading to a mixture of different compounds. Furthermore, the size of the molecule is beyond the reach of high-level computation. Therefore, we targeted investigations of a series of model compounds **2 – 4** (Scheme 2), containing *N,N*-dialkylaniline donor and TEE acceptor moieties. In contrast to **1**, *trans – cis* photoisomerization of the model compounds is a degenerate process leading to the starting material only.

Herein, we report the synthesis and photophysical properties of compounds **2 – 4**. The data obtained from the photophysical measurements are compared to a series of quantum chemical calculations. The focus in these calculations was on the ground and excited-state potential energy surfaces (PESs) and the fluorescence properties. For the computations, time-dependent density functional theory (TDFT) was mainly used. Even though the evaluation of vertical electronic excitation energies using Kohn – Sham response theory is well established,[15, 16] it is not until recently that implementations of the TDFT method in
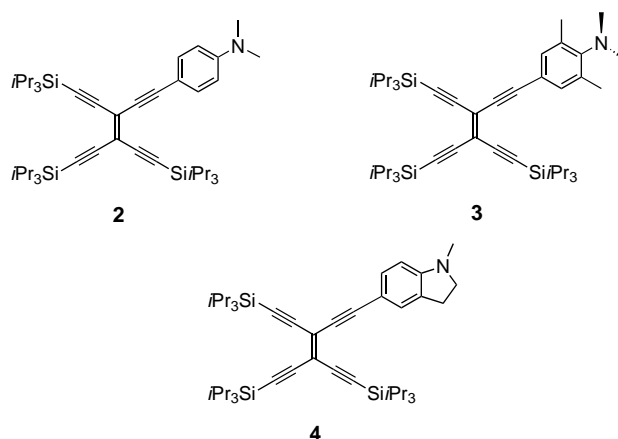
Scheme 2. *Donor – acceptor derivatives 2 – 4 with N,N-dialkylaniline donor and tetraethynylethene acceptor moieties investigated in this study.*

computer application programs became available. It has been shown that the method gives excitation energies that compare very well with the best ab initio methods available (see for example refs. [17, 18]).

Both experimental and computational data support a TICT model to explain the photophysical properties of *N,N*-dialkylaniline – TEE donor – acceptor conjugates. In compound **2** the Me_2N as well as the entire DMA group can undergo rotation (see Figure 8), thus potentially allowing two different TICT states. We therefore use the term TICT not only for CT states formed upon rotation about the nitrogen – phenyl bond but also for CT states formed upon rotation about other kinds of bonds.
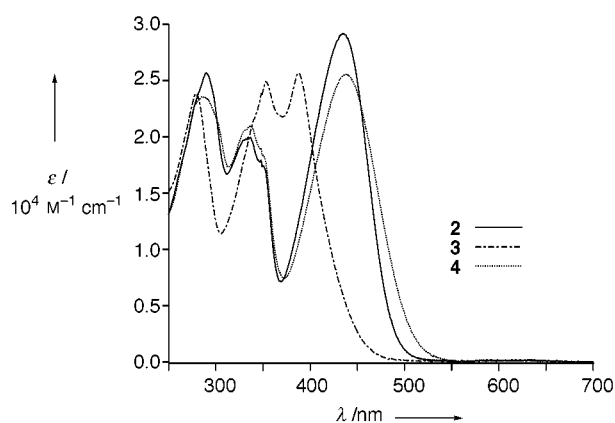
Results and Discussion

Synthesis

Compounds **2 – 4** were prepared starting from the 4-iodoaniline derivatives **5 – 7**, which were coupled to TEE **8**[1b] using the Pd^0-catalyzed Shonogashira cross-coupling reaction (Scheme 3). They are stable solids which were fully characterized spectroscopically and gave correct elemental analyses. For comparison, phenylated **9** was also prepared starting from TEE **10**[5c] and iodobenzene.

Absorption and Emission Spectroscopy

The electronic absorption spectra of the three model compounds **2 – 4** were recorded from CH_2Cl_2 solutions (Figure 1). The spectra of **2** and **4** are very similar, with the longest-wavelength absorption maxima appearing at $\lambda_{max} = 434$ and 438 nm, respectively. These results are in accord with the nearly identical planar conjugated π-systems in both compounds. Because of the steric hindrance arising from the two additional *o*-methyl groups, the dimethylamino group in **3** is twisted out of the TEE plane with the lone pair orbital of the nitrogen atom nearly orthogonal to the residual aryl – TEE π-system. As a result of this deconjugation, the longest-wavelength absorption maximum of **3** is significantly shifted to higher energy ($\lambda_{max} = 388$ nm) and the
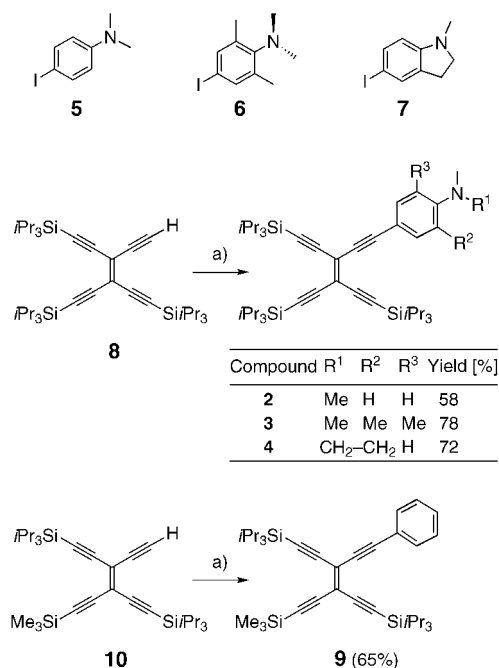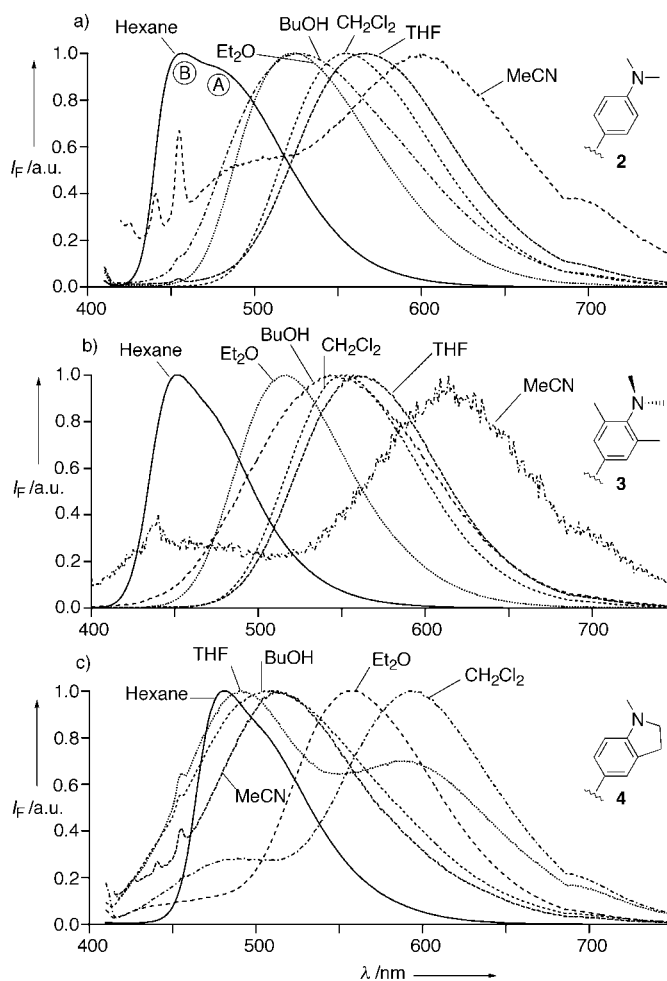
Scheme 3. *Synthesis of the donor–acceptor derivatives **2–4** and comparison compound **9**. a) **5**, **6**, **7**, or iodobenzene, [PdCl$_2$(PPh$_3$)$_2$], CuI, iPr$_2$NH, THF, 20 °C, 6.5 h.*

Figure 1. *Electronic absorption spectra of **2–4** in CH$_2$Cl$_2$ at 20 °C.*

Figure 2. *Normalized emission spectra of **2–4** in different solvents at 20 °C. a) [**2**] = 2.08 × 10^{-5} M; b) [**3**] = 2.65 × 10^{-5} M; c) [**4**] = 2.51 × 10^{-5} M). A and B in the spectrum of **2** in hexane are labels for the emission bands.*

fluorescence of all three compounds is characterized by an increase in Stokes shift with increasing solvent polarity (Table 1). This is in accordance with the polar nature of the emitting excited states, that involves a charge transfer from the dialkylaniline donor to the TEE acceptor. The dependence of the Stokes

overall UV/Vis spectrum resembles the one of the phenylated TEE **9** (UV/Vis bands in **3**: $\tilde{\nu}_{max}$ (ε) = 35.8 (23 800), 28.3 (24 900), 25.8 (25 600); in **9**: 36.2 (20 000), 27.8 (31 000), 26.5 × 10^3 cm^{-1} (32 700 M^{-1} cm^{-1})). The strong similarity between their spectra suggests a similar nature for the vertically excited states of the two compounds. Clearly, intramolecular donor–acceptor interactions are effective in **2** and **4**, thereby inducing a bathochromic shift of the longest-wavelength absorption maximum, whereas such interactions only partly operate in **3** due to the sterically enforced deconjugation of the Me$_2$N donor group.

The electronic emission spectra of **2–4** were recorded in solvents of different polarity (hexane, Et$_2$O, tetrahydrofuran (THF), CH$_2$Cl$_2$, MeCN, and BuOH). In contrast to the UV/Vis spectra, compounds **2** and **3** behave very similarly, while the fluorescence of **4** shows different features (Figure 2). The

Table 1. *Emission maxima$^{[a]}$ of **2–4** in various solvents and the solvent polarity parameter Δf.$^{[19]}$*

| Solvent | **2** | | **3** | | **4** | | |
	λ_{max} [nm]	$\tilde{\nu}_{max}$ [10^3 cm^{-1}]	λ_{max} [nm]	$\tilde{\nu}_{max}$ [10^3 cm^{-1}]	λ_{max} [nm]	$\tilde{\nu}_{max}$ [10^3 cm^{-1}]	Δf
Hexane	457$^{[b]}$/476$^{[c]}$	21.9/21.0	450	22.2	470	21.3	0.00
Et$_2$O	525	19.0	517	19.3	556	18.0	0.16
THF	565	17.7	560	17.9	491/592	20.4/16.9	0.21
CH$_2$Cl$_2$	554	18.0	552	18.1	489/593	20.4/16.9	0.22
MeCN	598	16.7	614	16.3	513	19.5	0.30
BuOH	529	18.9	543	18.4	518	19.3	0.26

[a] These values were obtained by deconvolution of the emission spectrum shown in Figure 2. Using the program *Origin*,$^{[20]}$ the experimental data were fitted by a function consisting of three Gaussian terms: $y = a_0 \exp\{-[(x-b_0)/c_0]^2\} + a_1 \exp\{-[(x-b_1)/c_1]^2\} + a_2 \exp\{-[(x-b_2)/c_2]^2\}$. [b] B-Band. [c] A-Band.

shift on solvent polarity was analyzed as described by Lippert.[19] In Equation (1), the solvent polarity parameter Δf is a function of the dielectric constant ε and refractive index n of the solvent.

$$\Delta f = \frac{\varepsilon - 1}{2\varepsilon + 1} - \frac{n^2 - 1}{2n^2 + 1} \tag{1}$$

The plot of the emission band maximum as a function of this parameter for a given compound should show a linear behavior if the same excited polar state is responsible for the emission in the different solvents. Such a linear relationship, Figure 3, was


a)

b)
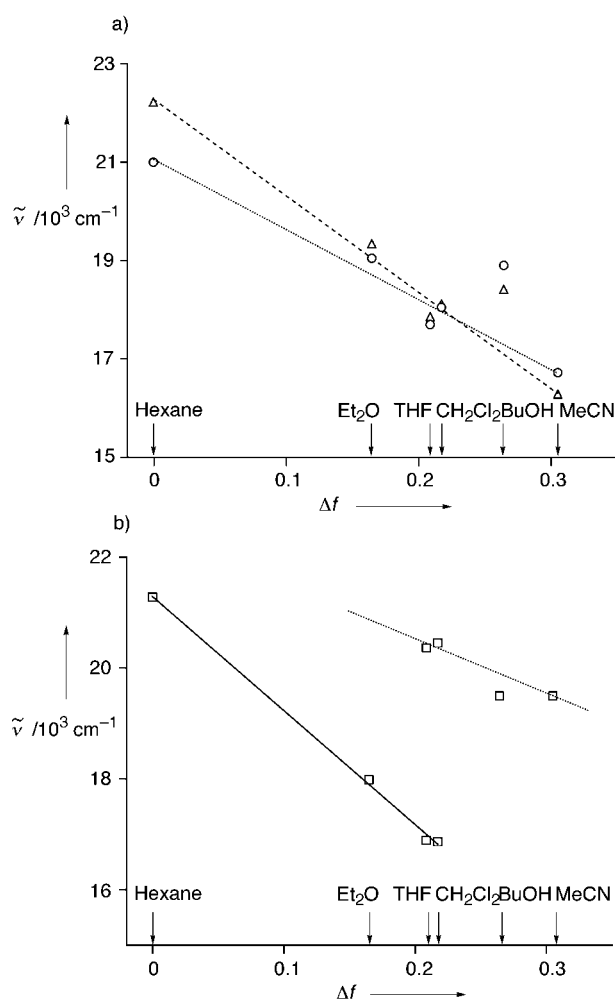
Figure 3. *Dependence of the emission maxima ($\tilde{\nu}$ [cm^{-1}]) of a) 2 ($\bigcirc$) and 3 ($\triangle$) and b) 4 from the solvent polarity parameter Δf. The values in BuOH were excluded from the linear regressions.*

indeed observed for **2** and **3**. The values recorded in BuOH must be excluded from the linear regression, as this protic solvent solvates the donor–acceptor chromophores not only through nonspecific weak apolar and polar contacts but also undergoes specific, directional hydrogen-bonding interactions with the solute. It is also known that the data recorded in THF are affected by additional weak specific interactions, thus always being slightly under the regression line.[12] The regression lines of **2** and **3** have very similar slopes (Figure 3a), which supports the

conclusion that the emitting excited states of these two systems are of the same kind.

A possible explanation for the observation of a dual fluorescence for **2** is the presence of an emitting TICT state. Next to the fluorescence from the CT state, characterized by the A-band at $\lambda_{max} = 476$ nm, an emission from the first excited state is observed in hexane for **2** (B-band, $\lambda_{max} = 457$ nm). The comparison of the absorption and emission spectra of **2** in hexane clearly demonstrates the $S_1 \rightarrow S_0$ transition character of this band (Figure 4). The photoexcitation of **3** does not directly lead to the emitting state but to a state higher in energy. Between the longest-wavelength absorption band ($\lambda_{max} = 388$ nm, 3.19 eV) and the A-band in the fluorescence spectrum ($\lambda_{max} = 552$ nm, 2.24 eV) in CH_2Cl_2, there is a gap of 0.95 eV (91.6 kJ mol^{-1}, Figure 4).

a)

b)
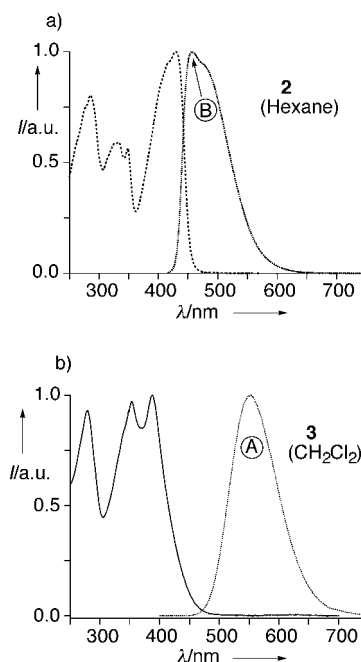
Figure 4. *Normalized electronic absorption and emission spectra of a) 2 in hexane and b) 3 in CH$_2$Cl$_2$.*

The polar nature of the first excited state of **2**, which is not found in compounds such as **3** and **9**, suggests a close relationship to the TICT state. The twisting reaction coordinate is more likely not related to a conical intersection with an energetically higher lying state (S_n), but takes place on a single potential hypersurface (S_1; Figure 5). Thus, the TICT state would represent a competitive channel to the ground state which could provide an attractive explanation for the failure of the DHA $\rightarrow$ VHF isomerization upon irradiation of **1**. This reaction channel seems to be quenched by the relaxation of the vertically excited singlet state to the emitting TICT state.

The dialkylamino group in **4** is unable to rotate; accordingly, a TICT state similar to those described above is not possible. The plot of the Stokes shifts versus Δf (Figure 3b) reveals the presence of two emitting excited states. The polarity of the surrounding solvent determines which state is preferred for the
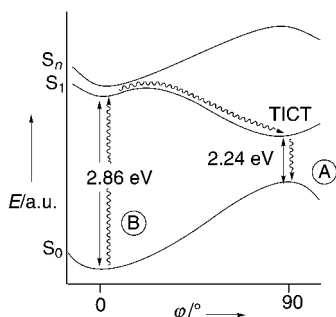
Figure 5. *Semiqualitative potential energy diagram for the twisting (angle φ [°]) of the dimethylamino group out of the plane of the arylated TEE in* **2** *in CH$_2$Cl$_2$. S$_1$ represents the "normal" first excited state that characterizes arylated TEEs, S$_n$ a higher excited state. The complete lack of the B-band in this solvent does not allow a quantitative picture. Energy conversions: 2.86 eV = 275 kJ mol^{-1}; 2.24 eV = 216 kJ mol^{-1}.*

emission. The jump from one emission state to the other takes place when the solvent polarity parameter reaches a value of $\Delta f \approx 0.21 - 0.22$. Both emissions are observed in THF ($\Delta f = 0.21$, $\lambda_1, \lambda_2 = 491, 592$ nm) and CH$_2$Cl$_2$ ($\Delta f = 0.22$, $\lambda_1, \lambda_2 = 489, 593$ nm). A TICT state in which the entire methylindolino group is twisted out of the plane of the TEE moiety might be responsible for one of the emissions (Figure 6). The presence of such a TICT state also finds support in the calculations described below. TICT states in which an entire *N,N*-dialkylanilino donor moiety is twisted out of the plane of the acceptor have been reported previously[21] (for further discussion, see refs. [22, 23]).
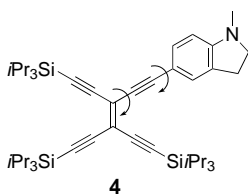
Figure 6. *Possible rotations about single bonds which could generate TICT states in* **4**.

Computational Studies

Methods

The quantum chemical computations of the ground- and excited-state properties of compounds **2–4** were performed using time-dependent density functional theory (TDFT; see ref. [15] for a review of the method) as implemented in the program Gaussian 98.[24] We used the B3LYP hybrid functional composed of the exchange functional of Becke[25] and the correlation functional of Lee, Yang, and Parr.[26] The 3-21G and 6-31G** Gaussian basis sets were used to represent the atomic orbitals.[27, 28]

Density functional theory is known to exaggerate the cumulenic character in polyactylenic compounds.[29] Optimized geometries using the Austin Model 1 (AM1)[30] often are in better agreement with experiment, an observation that appears to hold also for the compounds considered in the present study. We

therefore decided to perform the TDFT computations using AM1 geometries, a computational model referred to as TDFT–B3LYP/6-31G**//AM1 or TDFT–B3LYP/3-21G//AM1 when using the smaller basis set. The use of AM1 geometries only has a minor effect on the computed excitation energies (for **2**, the differences are 6 nm for the small basis set and less than 1 nm for the bigger basis set), and use of this model is motivated by computational efficiency rather than by accuracy considerations.

In the present study, we do not apply any corrections for solvent effects. Unlike in DMABN and many other compounds, the states involved in TICT channels are always the first allowed excitations, and as these are strongly polar it is very unlikely that solvent effects will invert the ordering of the excited states. We also have to point out that even the 6-31G** basis set, due to the lack of diffuse functions, will not allow a description of Rydberg states. We anticipate, however, that these are not of importance in the present context.

Computational Details and Results

In order to validate the computational model used, we first computed the electronic absorption bands of compounds **2–4**. In Table 2, the calculated and experimental longest-wavelength

Table 2. *Comparison of the computed and experimental (in hexane) longest-wavelength absorption maxima, the composition of the absorption bands,*[a] *and the oscillator strength.*

Compound	Experimental λ_{max} [nm]	Computed values[b]		
		λ_{max} [nm]	Oscillator strength[c]	Composition of band/ CI coefficients[d]
2	434	(420)	(0.76)	H-1 →L 0.15
		425	0.80	H →L 0.63
3	388	(363)	(0.86)	H-3 →L -0.16
		377	0.80	H-1 →L 0.60
4	438	(439)	(0.72)	H-1 →L 0.14
		444	0.72	H →L 0.63

[a] The absorption bands are characterized by the configuration interaction (CI) expansion coefficients of the dominant excitations. The absorption spectrum was computed using the TDFT–B3LYP/6-31G**//AM1 model. [b] Values in parenthesis refer to absorption wavelengths and oscillator strength computed using the smaller basis set TDFT–B3LYP/3-21G//AM1 model. [c] Arbitrary units. [d] H and L refer to HOMO and LUMO, respectively.

absorption maxima are compared. The TDFT–B3LYP/6-31G**//AM1 calculations predict the first absorption for compounds **2** and **4** to occur at 425 and 444 nm, respectively (experimental values in hexane: 434 and 438 nm). The first absorption for **3** is correctly predicted to occur at a shorter wavelength, namely at 377 (388 nm). Using the smaller 3-21G basis set, we observe a somewhat larger discrepancy between computation and experiment, but the relevant qualitative features, such as the blue shift observed for the longest-wavelength absorption band of **3**, are still correctly reproduced. The largest deviations between computed and experimental absorption energies, as measured for the three compounds in hexane, are 0.1 (6-31G*) and 0.23 eV (3-21G). For compound **2** the deviations are 0.06 (6-31G*) and

0.09 eV (3-21G), respectively. We should point out that here we are comparing data representing vertical excitations without zero-point energy corrections (TDFT) with Franck–Condon transitions (experiment).

Even though it has been observed that the TDFT method may fail in situations with considerable charge transfer,[31] the results of the electronic absorption calculations as well as the results of similar studies on other charge-transfer compounds, such as aminobenzonitrile and derivatives,[32] show that there is reasonable agreement with the experimental spectra. The computational model chosen appears to be appropriate for the investigation of the spectral properties of the donor–acceptor compounds **2** – **4**. For purely qualitative predictions, even the small 3-21G basis set may be adequate.

Table 2 shows that for **2** and **4** the first excitation is primarily composed of an electronic transition from the HOMO to the LUMO (H →L excitation). Figure 7 confirms that these are in fact charge-transfer excitations. Accordingly, the dipole moment for the excited state is 25.6 and 27.1 Debye, respectively (TDFT using the 3-21G basis set). In **3**, however, the HOMO shows less amplitude on the DMA group (Figure 7b). In this case, the excitation has a strong component which is of TEE $\pi \rightarrow \pi^*$ character.

In the twisted compound **3**, the donor effect of the Me$_2$N group, namely the antibonding interaction between the nitrogen lone-pair and the π-system of the phenyl ring, is reduced, thus, relative to the HOMOs of **2** and **4** the HOMO of **3** is more stable. The LUMOs of all three compounds, on the other hand, have the same shape and orbital energies, with the charge located essentially on the TEE unit. The blue shift observed in the absorption spectrum of **3** can thus be related to the lower energy of its HOMO.
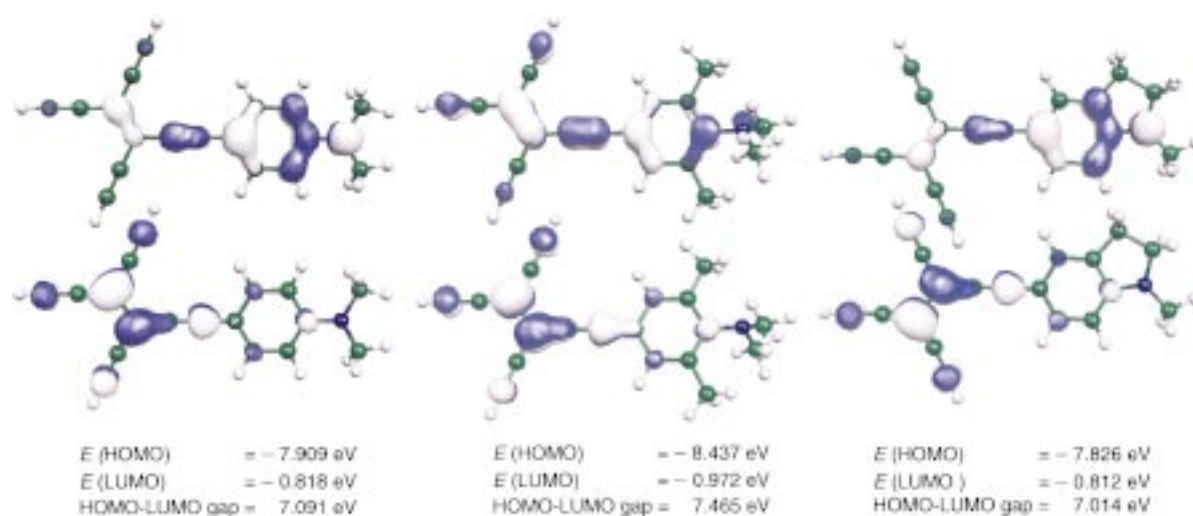
The hypothesis of a TICT state was further investigated by performing TDFT–B3LYP/3-21G//AM1 model calculations. The computational strategy was to follow the rotation of the Me$_2$N group about the N—C$_{phenyl}$ single bond, the rotation of the DMA group about the C$_{phenyl}$—C$_{TEE}$ single bond, as well as the rotation

about the central TEE double bond. All other structural parameters were kept at their ground-state values, that is, the electronically excited-state potential energy surface (PES) was probed only along these three specific coordinates with no relaxation of any other geometric parameters. A systematic search of excited-state potential energy surfaces is difficult to perform as to date the nuclear gradient computation for TDFT is not yet commonly available.
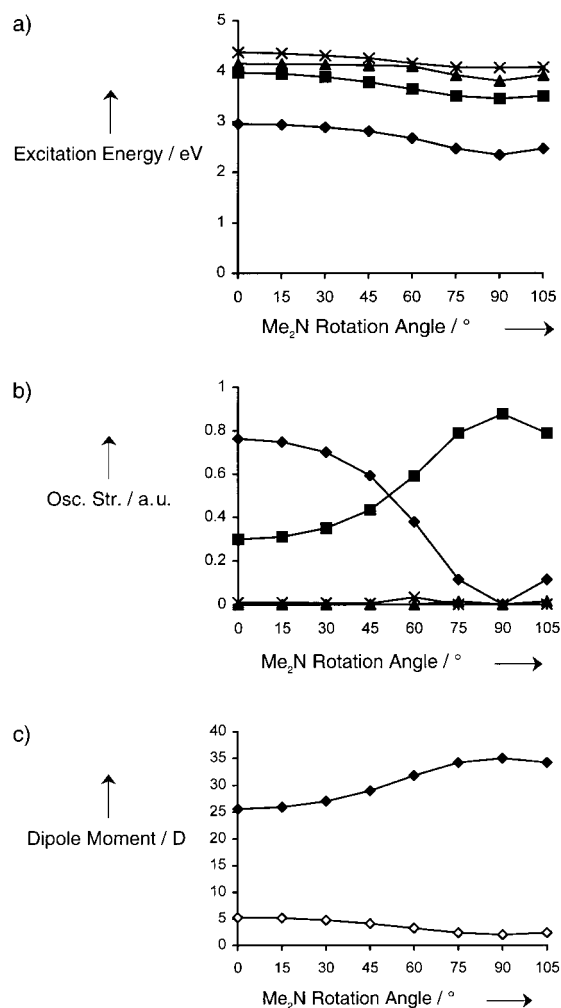
The excitation energies of the first four singlet excited states and the corresponding oscillator strength and dipole moments as a function of the angle of rotation of the Me$_2$N and DMA moieties were evaluated as shown in Figures 8 and 9. We observe that for both rotations the lowest singlet excited state shows a minimum of the excitation energy, a maximum for the dipole moment, and zero oscillator strength at a torsional angle $\tau = 90°$. This particular point also represents a minimum on the S$_1$ excited-state surface. The loss of oscillator strength and the gain in dipole moment while relaxing to a twisted conformation are part of the characteristics of a TICT state. For both rotation coordinates, only the lowest excited state shows TICT character.

The results for the rotation about the central TEE double bond are summarized in Figure 10. Along this reaction coordinate, we observe a crossing of the S$_0$ and S$_1$ PESs for $\tau = 90°$, thus representing a radiationless transition channel. The minimum found with the 90° twisted TEE double bond also represents the lowest energy point of this excited surface identified so far.

In Figure 11, all the potential energy surfaces along all three reaction coordinates for the first excited state are collected into one diagram for compound **2**. For all three rotation coordinates, we find a minimum at $\tau = 90°$. For the rotation of the DMA group, the potential energy curve is monotonously falling, whereas for the rotation of the Me$_2$N group we first observe a slight increase of the potential energy, followed by a steady descent to the minimum at $\tau = 90°$. An even higher barrier is observed for the rotation about the central double bond of the TEE unit. We have to point out that these PESs were obtained from calculations that only varied the angle of rotation about the
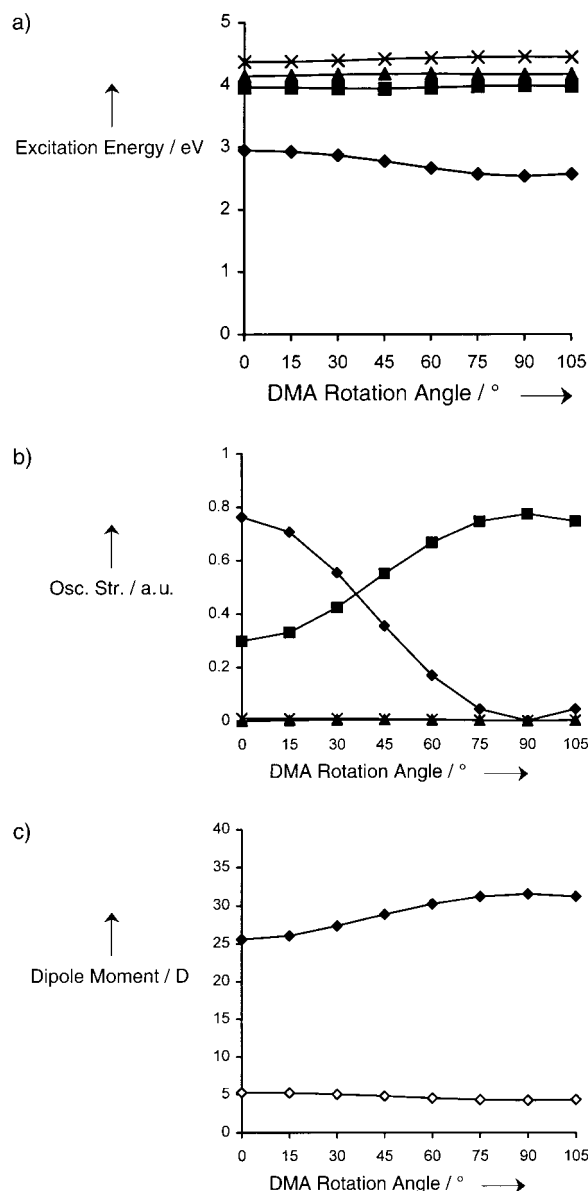

E (HOMO) = – 7.909 eV	E (HOMO) = – 8.437 eV	E (HOMO) = – 7.826 eV
E (LUMO) = – 0.818 eV	E (LUMO) = – 0.972 eV	E (LUMO) = – 0.812 eV
HOMO-LUMO gap = 7.091 eV	HOMO-LUMO gap = 7.465 eV	HOMO-LUMO gap = 7.014 eV

Figure 7. Structures and energies of the HOMO and the LUMO of compounds a) 2, b) 3, and c) 4, as computed using the TDFT – B3LYP/6 – 31G**//AM1 model (see text for discussion of the orbital features). The top structure always represents the HOMO, the bottom one the LUMO.

Figure 8. *The a) excitation energy and b) oscillator strength for the first four singlet excited states of compound **2** as a function of the angle of rotation of the Me_2N group about the $N\!-\!C_{phenyl}$ single bond using the TDFT – B3LYP/3-21G//AM1 model. c) The dipole moment is shown for the ground and the first excited state only. Note that even though the excitation energy is steadily decreasing, the energy of the emitting state is not (see Figure 11). Symbols: $\diamond$ indicates S_0, $\blacklozenge$ S_1, $\blacksquare$ S_2, $\blacktriangle$ S_3, and $\times$ S_4.*

Figure 9. *The a) excitation energy and b) oscillator strength for the first four singlet excited states of compound **2** as a function of the angle of rotation of the DMA group about the $C_{phenyl}\!-\!C_{TEE}$ single bond using the TDFT – B3LYP/3-21G//AM1 model. c) The dipole moment is shown for the ground and the first excited state. Symbols: $\diamond$ indicates S_0, $\blacklozenge$ S_1, $\blacksquare$ S_2, $\blacktriangle$ S_3, and $\times$ S_4.*

respective bonds specified above. All other geometrical parameters were kept fixed at their ground-state values. The barriers of 0.18 and 0.4 eV predicted for the rotation of the Me_2N group and for the rotation about the TEE double bond, respectively, might therefore be drastically reduced or even disappear when additional parts of or the entire structure is allowed to relax. In a recent paper,[33] Mennucci et al. showed that in DMABN the minimum energy path connecting the LE state with the TICT state does not strictly follow the rotation coordinate but rather a coordinate that involves some wagging of the Me_2N methyl groups.

In the case of either Me_2N or DMA rotation, it is the *first* excited state which shows TICT character. The calculations further support the view, already expressed above when discussing the experimental results, that along the twisting reaction coordinate there is no conical intersection with an energetically higher-lying state, and that therefore the fluorescence process
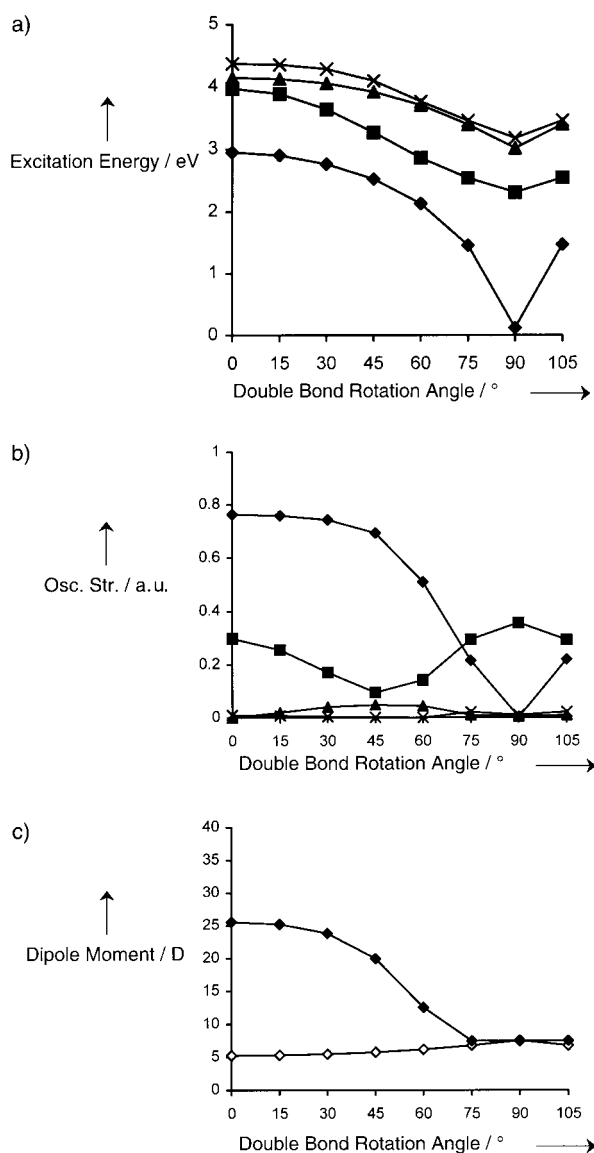
takes place on a single potential energy surface (see also Figure 5).

The calculations predict the emission energy of the A-band of **2** to be red shifted by 0.62 eV relative to the absorption energy if the emission is from the TICT state obtained by rotation of the Me_2N group. If the emission is from the TICT state resulting from the twisting of the DMA group, the computed red shift is 0.41 eV with a predicted wavelength for the emission of 490 nm (see Figure 11). This value is between the values observed for the A-band in hexane (476 nm) and in Et_2O (525 nm). For compound **2**, based on these calculations, there is the option for emission from two different TICT channels belonging to the same excited state. The calculated excited-state surface, however, is not
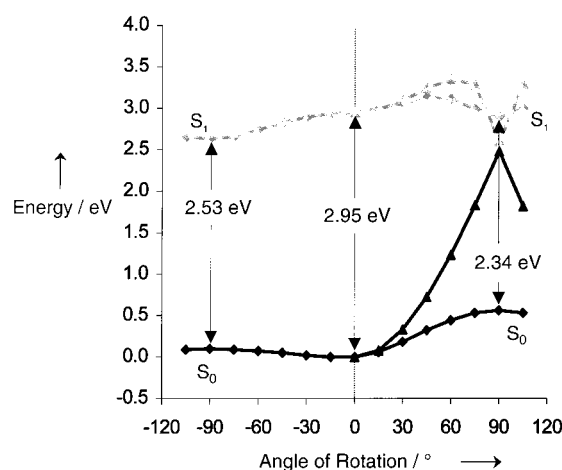
a)

b)

c)

Figure 10. *The a) excitation energy and b) oscillator strength for the first four singlet excited states of compound **2** as a function of the angle of rotation about the central TEE double bond using the TDFT – B3LYP/3-21G//AM1 model. c) The dipole moment is shown for the ground and the first excited state only. Note that even though the excitation energy is steadily decreasing, the energy of the emitting state is not (see Figure 11). Symbols: ◇ indicates S_0, ◆ S_1, ■ S_2, ▲ S_3, and ✕ S_4.*

Figure 11. *The (one-dimensional) potential energy surfaces for the ground and first excited state of compound **2** along all three rotation coordinates using the TDFT – B3LYP/3-21G//AM1 model. Ground-state energies are represented with black lines, excited-state energies with gray. Energies computed for the rotation of the Me_2N group and the DMA group are indicated with ◆, whereas energies computed for the rotation about the central TEE double bond are marked with ▲. In addition, for clarity, the rotation of the DMA group is plotted for negative rotation angles (left side of the chart). The Figure shows the minimum of the first excited state PES at $\tau = 90°$ for the twisting of the Me_2N and DMA groups. At the same angle, we also observe the crossing of the potential curves for the rotation about the TEE double bond (radiationless transition).*
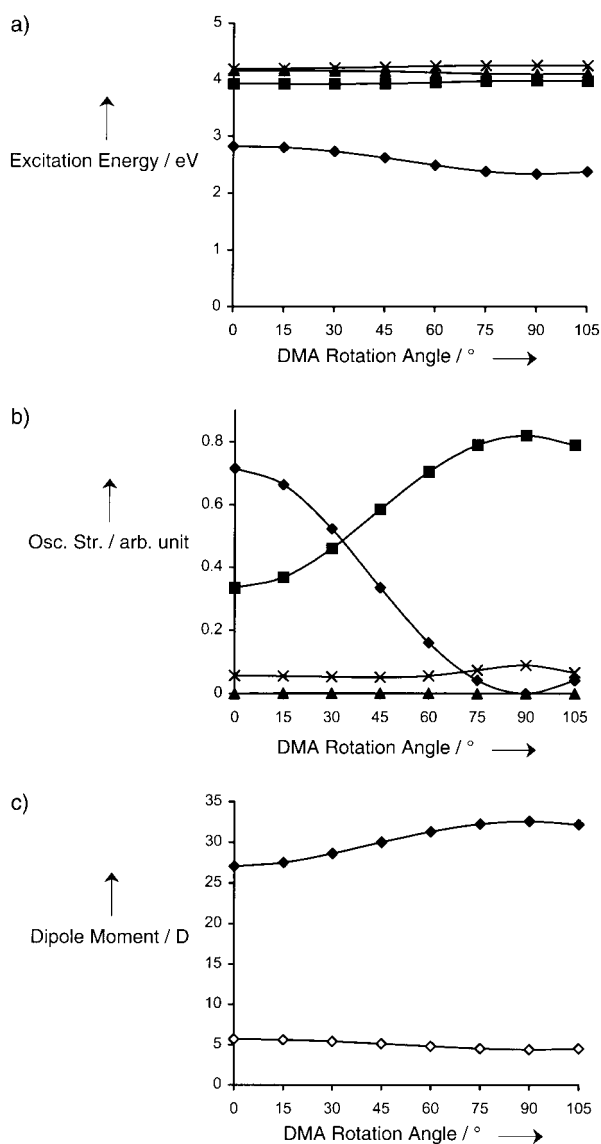
(556 nm), the shortest-wavelength emission measured for **4** that most probably is of A-band type.

From the experiments, based on the analysis of the dependence of the emission maxima on solvent polarity, indications are that the A-band emissions observed are due to two different charge-transfer states (Figure 3). From the present computations, we learn that at least one of the CT states responsible for the A-band is of the TICT type. In order to further pursue the question of the nature of the second emitting state, we will need to perform more elaborate calculations (better basis sets, more extensive scan of the S_1 surface), and we will also have to include solvent effects in our computational model, similar to the work presented by Mennucci et al. on TICT states in DMABN.[33] We will also need to perform further experimental investigations in order to be able to reach more definite conclusions.

Conclusions

This work establishes the role of DMA – TEE conjugates as a new class of donor – acceptor compounds possessing an emitting CT state. The experimental data indicate that the first excited state of **2** possesses a reaction coordinate related to a twist of the dimethylamino group leading to a TICT state. Similar emitting properties of **2** and **3**, in which the dimethylamino group is forced into orthogonality with respect to the adjacent phenyl group, tend to support this conclusion. In **4**, the rotation of the dialkylamino group is not possible but a similar TICT state is reached, presumably by rotation of the entire methylindolino group out of the TEE acceptor plane. Compounds **2** – **4** were prepared as model compounds for the three-way chromophoric switch **1** which failed to undergo photochemical dihydro-

accurate enough to assess which of the two channels is the preferred one.

In compound **4**, the dialkylamino group is locked in plane by incorporation into the five-membered ring structure and, therefore, only the entire methylindolino group is free to rotate. As in **2**, we observe a steady energy decrease from the initial excited state along the twisting coordinate to a minimum at $\tau = 90°$ (Figure 12). Again, we observe an increase of the dipole moment and a decrease of the transition dipole along the twisting coordinate. The calculations thus predict an A-band, which is due to a TICT state and which is red shifted by 0.49 eV from the absorption, placing the emission wavelength at 532 nm. This wavelength is somewhat shorter than the one observed in Et_2O

a)

b)

c)

Figure 12. *The a) excitation energy and b) oscillator strength for the first four singlet excited states of compound 4 as a function of the angle of rotation of the methylindolino group using the TDFT–B3LYP/3-21G//AM1 model. c) The dipole moment is shown for the ground and the first excited state only. The ground-state energy (not shown) only varies very little along the rotation coordinate (from 0.0 to 3.6 kJ mol^{-1} at $\tau = 90°$). Therefore, the excited-state curves can also be viewed as excited-state potential energy curves. Symbols: $\diamond$ indicates S_0, $\blacklozenge$ S_1, $\blacksquare$ S_2, $\blacktriangle$ S_3, and $\times$ S_4.*

azulene →vinylheptafulvene isomerization. The data suggest that this reaction channel of **1** is quenched by the efficient relaxation of the vertically excited singlet state to an emitting TICT state.

TDFT computations confirmed that the vertical excitation in compounds **2** and **4** is related to a charge transfer from the DMA group to the TEE moiety and that both compounds can relax to minima on the excited-state surface by twisting either the dimethylamino (in **2**) or the entire dialkylanilino donor group (in **2** or **4**) into a position perpendicular to the TEE acceptor. These minima are directly connected with the locally excited state, namely there is no crossing with other singlet surfaces involved.

From these minima, we predict emissions (A-band) that are close in energy to those observed experimentally in nonpolar solvents. The calculations thus show strong evidence for the presence of a TICT state for these two compounds.

In the DMA–TEE conjugate **2**, the Me$_2$N substituent is free to rotate. However, the calculations indicate that also in **2** the A-band emission arises from the minimum on the excited-state surface that is due to rotation of the entire DMA group. Along this coordinate, a barrier-free connection is observed between the locally excited state and the minimum on the surface from where the emission occurs. For an A-band due to rotation of the Me$_2$N substituent only, we predict a wavelength significantly longer than the experimental value in nonpolar solvents. We also observe a barrier of about 0.2 eV along that coordinate. Thus, experiment and calculation tend to disagree on whether the entire DMA group or only the Me$_2$N moiety is twisted in the emitting TICT state in **2**.

In compound **4**, the analysis of the dependence of the emission maxima on solvent polarity indicated that the A-band is due to more than one emitting state. Without explicit consideration of solvent effects and, without an extended search on the excited-state surface, we are not in a position to provide a sound theoretical argument regarding the nature of the second emitting state. It is very likely, however, that one of the emitting states is a TICT state. The second emission might be form a minimum on the excited-state surface where the molecule retains planarity but adopts a highly polar resonance structure (for example, a quinoid–cumulenic structure with a planar Me$_2$N group). Such structures have been observed for the anions of TEE-based donor–acceptor systems.[6]

Experimental Section

Solvents and reagents were reagent-grade and used without further purification unless otherwise stated. THF and Et$_2$O were freshly distilled from sodium benzophenone ketyl. Compounds **5**,[34] **8**,[1b] and **10**[5c] were prepared according to literature procedures.

The electronic absorption spectra were recorded on a Varian Cary 5 UV/Vis/NIR spectrophotometer. For the electronic emission spectroscopy studies, a Spex 1680 0.22 m double spectrometer was used. The spectra were run in quartz cuvettes with a width of 1.0 cm. The excitation wavelength was of 400 nm for **2** and **4** and of 390 nm for **3**.

1-[4-(Dimethylamino)phenyl]-3,4-bis[(triisopropylsilyl)ethynyl]-6-(triisopropylsilyl)hex-3-ene-1,5-diyne (**2**). To a degassed solution of **8** (213 mg, 0.36 mmol) and **5** (96 mg, 0.39 mmol) in THF (10 mL), a degassed mixture of [PdCl$_2$(PPh$_3$)$_2$] (8 mg, 0.012 mmol) and CuI (4 mg, 0.02 mmol) in THF (10 mL) and iPr$_2$NH (5 mL) was added. After stirring under N$_2$ for 6.5 h, aqueous workup afforded the crude product, that was purified by column chromatography (SiO$_2$-60 (50 g); hexane/ CH$_2$Cl$_2$ 3/1). Yield: 160 mg (58%). Orange solid; m.p. 141–142 °C; ^{1}H NMR (200 MHz, CDCl$_3$): $\delta = 1.16$ (s; 63 H), 3.05 (s; 6H), 6.66 (d, $J = 8.1$ Hz; 2H), 7.37 (d, $J = 8.1$ Hz; 2H); ^{13}C NMR (75 MHz, CDCl$_3$): $\delta = 11.28$, 18.65, 40.11, 86.97, 100.72, 100.85, 100.91, 101.40, 104.00, 104.29, 104.47, 109.44, 111.56, 114.39, 118.17, 133.14, 150.45; IR (KBr): $\tilde{\nu} = 2942$ (s), 2864 (s), 2191(m), 2141 (m), 1609 (s), 1532 (m), 1463 (m), 1372 (w), 1148 (m), 1025 (m), 883 (m), 810 cm^{-1} (m); UV/Vis (CH$_2$Cl$_2$): 290 (25 700), 337 (19 900), 350 (sh, 17 400), 434 nm (29 200 M^{-1} cm^{-1}); FAB-MS: $m/z = 1423.8$ (11, M_2^+), 1380.8 (5, $[M_2 - i$Pr$]^+$), 818.5 (15),

711.5 (100, M^+); elemental analysis for $C_{45}H_{73}NSi_3$ (712.32): calcd C 75.88, H 10.33, N 1.97; found C 75.97, H 10.21, N 1.93.

1-[4-(Dimethylamino)-3,5-dimethylphenyl]-3,4-bis[(triisopropylsilyl)-ethynyl]-6-(triisopropylsilyl)hex-3-ene-1,5-diyne (3). Compound **3** was prepared according to the procedure for **2**, starting from **5** (320 mg, 0.54 mmol) and **7** (178 mg, 0.65 mmol). Yield: 312 mg (78%). Yellow resin that crystallized after several days; m.p. 96 °C; ^1H NMR (300 MHz, CDCl$_3$): $\delta = 1.09$ (s; 21 H), 1.11 (s; 21 H), 1.11 (s; 21 H), 2.24 (s; 6 H), 2.81 (s; 6 H), 7.09 (s; 2 H); ^{13}C NMR (75 MHz, CDCl$_3$): $\delta = 11.19$, 11.22, 18.55, 18.87, 42.31, 87.28, 99.31, 101.27, 101.62, 101.96, 103.84, 104.19, 104.37, 116.07, 117.90, 118.53, 132.46, 136.78, 151.11; IR (KBr): $\tilde{v} = 2942$ (s), 2864 (s), 2196 (w), 2150 (w), 1463 (m), 1214 (m), 1159 (w), 1120 (m), 1055 (m), 1018 (w), 994 (m), 958 (w), 881 cm^{-1} (m); UV/Vis (CH$_2$Cl$_2$): 279 (23 800), 353 (24 900), 388 nm (25 600 M^{-1} cm^{-1}); FAB-MS: $m/z = 739.6$ (100, M^+), elemental analysis for $C_{47}H_{77}NSi_3$ (740.39): calcd C 76.25, H 10.48, N 1.89; found C 76.18, H 10.44, N 1.95.

1-Methyl-5-{6-(triisopropylsilyl)-3,4-bis[(triisopropylsilyl)ethynyl]hex-3-ene-1,5-diynyl}indoline (4). Compound **4** was prepared according to the procedure for **2**, starting from **5** (285 mg, 0.48 mmol) and **8** (124 mg, 0.48 mmol). Yield: 249 mg (72%). Red resin that slowly solidified; m.p. 136 – 138 °C; ^1H NMR (300 MHz, CDCl$_3$): $\delta = 1.09$ (s; 21 H), 1.10 (s; 21 H), 1.11 (s; 21 H), 2.79 (s; 3 H), 2.93 (t, $J = 8.3$ Hz; 2 H), 3.39 (t, $J = 8.3$ Hz; 2 H), 6.34 (d, $J = 8.1$ Hz; 1 H), 7.13 (s; 1 H), 7.20 (s; 1 H); ^{13}C NMR (75 MHz, CDCl$_3$): $\delta = 11.30$, 18.65, 28.01, 34.93, 55.30, 86.56, 100.59, 100.81, 101.27, 101.49, 103.97, 104.36, 104.58, 105.83, 110.49, 114.31, 118.19, 127.74, 129.97, 132.43, 153.83; IR (KBr): $\tilde{v} = 2942$ (s), 2864 (s), 2187 (m), 2141 (m), 1613 (s), 1514 (m), 1463 (m), 1384 (m), 1313 (m), 1170 (m), 1020 (m), 883 cm^{-1} (m); UV/Vis (CH$_2$Cl$_2$): 286 (23 600), 337 (21 000), 350 (sh, 18 400), 438 nm (25 500 M^{-1} cm^{-1}); FAB-MS: $m/z = 1446.9$ (13, M_2^+), 723.6 (100, M^+); elemental analysis for $C_{46}H_{73}NSi_3$ (724.35): calcd C 76.28, H 10.16, N 1.93; found C 76.32, H 10.18, N 2.12.

4-(Dimethylamino)-3,5-dimethyliodobenzene (6). A solution of 4-(dimethylamino)-3,5-dimethylbromobenzene[35] (1.00 g, 4.38 mmol) in THF (45 mL) under N$_2$ was cooled to −78 °C, and 1.6 M BuLi (6.85 mL, 10.9 mmol) in hexane was added. After stirring for 1 h at −78 °C, I$_2$ (2.78 g, 10.9 mmol) in THF (45 mL) was added. The mixture was stirred for 15 min, then 1 M aq. Na$_2$S$_2$O$_3$ (10 mL) was added. After warming to 20 °C, aq. workup and distillation (140 °C, 7 Torr) afforded pure **6** (803 mg, 67%) besides 202 mg (17%) of product containing traces of 2,5,N,N-tetramethylaniline. Colorless oil; b.p. 140 °C/7 Torr; ^1H NMR (200 MHz, CDCl$_3$): $\delta = 2.23$ (s; 6 H), 2.78 (s; 6 H), 7.32 (s; 2 H); ^{13}C NMR (75 MHz, CDCl$_3$): $\delta = 18.55$, 42.15, 89.25, 137.44, 139.45, 149.56; IR (CHCl$_3$): 2922 (m), 2778 (m), 1561(w), 1473 (s), 1328 (w), 1146 (s), 1100 cm^{-1} (w); EI-MS: 275.0 (100, M^+), 260.0 (64, [M − CH$_3$]$^+$), 243.9 (38). HR-EI-MS: $m/z = 275.0170$ (M^+); calcd for $C_{10}H_{14}NI$: 275.0173.

5-Iodo-1-methylindoline (7). To 1-methylindoline[36] (1.00 g, 7.51 mmol) and CaCO$_3$ (977 mg, 9.76 mmol) in CH$_2$Cl$_2$ (100 mL) and MeOH (40 mL), benzyltrimethylammonium dichloroiodate[37] (2.61 g, 7.51 mmol) was added and the mixture was stirred for 45 min. The remaining CaCO$_3$ was filtered, the solvent evaporated, and the residue dissolved in Et$_2$O (100 mL). The org. phase was washed with 1 M aq. Na$_2$S$_2$O$_3$ (50 mL) and H$_2$O (50 mL) and dried (MgSO$_4$). Evaporation of the solvent afforded **7** (1.79 g, 92%) as an unstable oil that had to be immediately stored at −20 °C. ^1H NMR (300 MHz, CDCl$_3$): $\delta = 2.75$ (s; 3 H), 2.94 (t, $J = 8.1$ Hz; 2 H), 3.32 (t, $J = 8.1$ Hz; 2 H), 6.27 (d, $J = 7.9$ Hz; 1 H), 7.34 (s; 1 H), 7.36 (d, $J = 7.9$ Hz; 1 H); ^{13}C NMR (75 MHz, CDCl$_3$): $\delta = 28.17$, 35.68, 55.69, 78.07, 108.90, 132.59, 132.95, 135.73, 152.86; IR (CHCl$_3$): $\tilde{v} = 3007$ (w), 2944 (w), 2814 (w), 1598 (m), 1490 (s), 1469 (s), 1378 (w), 1312 (m), 1264 (m), 1091 cm^{-1} (m); EI-MS:

259.0 (100, M^+), 131.1 (55), 117 (14). HR-EI-MS: $m/z = 258.9857$ (M^+); calcd for $C_9H_{10}NI$: 258.9860.

(E)-1-Phenyl-3,4-bis[(triisopropylsilyl)ethynyl]-6-(trimethylsilyl)hex-3-ene-1,5-diyne (9). Compound **9** was prepared following the procedure for **2**, starting from **10** (315 mg, 0.62 mmol) and iodobenzene (0.14 mL, 243 mg, 1.24 mmol). Yield: 235 mg (65%). Orange crystals; m.p. 67 °C; ^1H NMR (200 MHz, CDCl$_3$): $\delta = 0.23$ (s; 9 H), 1.12 (s; 21 H), 1.15 (s; 21 H), 7.31 – 7.37 (m; 3 H), 7.45 – 7.72 (m; 2 H); ^{13}C NMR (50 MHz, CDCl$_3$): $\delta = -0.36$, 11.25, 11.32, 18.59, 18.71, 87.44, 98.52, 101.86, 102.14, 102.33, 103.32, 103.82, 104.65, 117.35, 117.92, 122.75, 128.24, 128.90, 131.82; IR (KBr): $\tilde{v} = 2943$ (s), 2863 (s), 2200 (w), 2133 (w), 1463 (m), 1252 (m), 1154 (m), 862 cm^{-1} (s); UV/Vis (CH$_2$Cl$_2$): 276 (20 000), 352 (sh, 30 300), 359 (31 000), 377 nm (32 700 M^{-1} cm^{-1}); EI-MS: $m/z = 584.4$ (100, M^+), 499.4 (37), 457.3 (41), 415.3 (57), 73.1 (25, [SiMe$_3$]$^+$); elemental analysis for $C_{37}H_{56}Si_3 \cdot$ MeOH (617.15): calcd C 75.95, H 10.07; found C 75.88, H 10.11.

[1] a) L. Gobbi, P. Seiler, F. Diederich, *Angew. Chem.* **1999**, *111*, 737 – 740; *Angew. Chem. Int. Ed.* **1999**, *38*, 674 – 678; b) L. Gobbi, P. Seiler, F. Diederich, V. Gramlich, C. Boudon, J.-P. Gisselbrecht, M. Gross, *Helv. Chim. Acta* **2001**, *84*, 743 – 777.

[2] a) F. Diederich in *Modern Acetylene Chemistry* (Eds.: P. J. Stang, F. Diederich), VCH, Weinheim, **1995**, pp. 443 – 471; b) R. R. Tykwinski, F. Diederich, *Liebigs Ann.* **1997**, 649 – 661; c) F. Diederich, L. Gobbi, *Top. Curr. Chem.* **1999**, *201*, 43 – 79.

[3] a) J. Daub, T. Knöchel, A. Mannschreck, *Angew. Chem.* **1984**, *96*, 980 – 981; *Angew. Chem. Int. Ed. Engl.* **1984**, *23*, 960 – 961; b) J. Daub, S. Gierisch, U. Klement, T. Knöchel, G. Maas, U. Seitz, *Chem. Ber.* **1986**, *119*, 2631 – 2646; c) S. Gierisch, W. Bauer, T. Burgemeister, J. Daub, *Chem. Ber.* **1989**, *122*, 2341 – 2349; d) J. Daub, J. Salbeck, T. Knöchel, C. Fischer, H. Kunkely, K. M. Rapp, *Angew. Chem.* **1989**, *101*, 1541 – 1542; *Angew. Chem. Int. Ed. Engl.* **1989**, *28*, 1494 – 1496; e) J. Achatz, C. Fischer, J. Salbeck, J. Daub, *J. Chem. Soc. Chem. Commun.* **1991**, 504 – 507; f) T. Mrozek, H. Görner, J. Daub, *Chem. Commun.* **1999**, 1487 – 1488.

[4] a) R. E. Martin, J. Bartek, F. Diederich, R. R. Tykwinski, E. C. Meister, A. Hilger, H. P. Lüthi, *J. Chem. Soc. Perkin Trans. 2* **1998**, 233 – 241; b) L. Gobbi, P. Seiler, F. Diederich, V. Gramlich, *Helv. Chim. Acta* **2000**, *83*, 1711 – 1723.

[5] a) J. Anthony, C. Boudon, F. Diederich, J. P. Gisselbrecht, V. Gramlich, M. Gross, M. Hobi, P. Seiler, *Angew. Chem.* **1994**, *106*, 794 – 798; *Angew. Chem. Int. Ed. Engl.* **1994**, *33*, 763 – 766; b) A. M. Boldi, J. Anthony, V. Gramlich, C. B. Knobler, C. Boudon, J. P. Gisselbrecht, M. Gross, F. Diederich, *Helv. Chim. Acta* **1995**, *78*, 779 – 796; c) R. R. Tykwinski, M. Schreiber, R. Pérez Carlón, F. Diederich, V. Gramlich, *Helv. Chim. Acta* **1996**, *79*, 2249 – 2281.

[6] A. Hilger, J. P. Gisselbrecht, R. R. Tykwinski, C. Boudon, M. Schreiber, R. E. Martin, H. P. Lüthi, M. Gross, F. Diederich, *J. Am. Chem. Soc.* **1997**, *119*, 2069 – 2078.

[7] Upon protonation of **1**, the fluorescence intensity decreases approximately by a factor of 300; see ref. [1].

[8] a) E. Lippert, W. Lüder, F. Moll, W. Nägele, H. Boos, H. Prigge, I. Seibold-Blankenstein, *Angew. Chem.* **1961**, *73*, 695 – 706; E. Lippert, W. Lüder, H. Boos in *Advances in Molecular Spectroscopy, Proceedings of the 4th International Meeting on Molecular Spectroscopy, Vol. 1* (Ed.: A. Mangini), Pergamon, Oxford, **1962**, pp. 443 – 457.

[9] W. Rettig, B. Bliss, K. Dirnberger, *Chem. Phys. Lett.* **1999**, *305*, 8 – 14.

[10] K. A. Zachariasse, *Chem. Phys. Lett.* **2000**, *320*, 8 – 13.

[11] a) Z. R. Grabowski, K. Rotkiewicz, A. Siemiarczuk, D. J. Cowley, W. Baumann, *Nouv. J. Chim.* **1979**, *3*, 443 – 454; b) K. Rotkiewicz, K. H.

Grellmann, Z. R. Grabowski, *Chem. Phys. Lett.* **1973**, *19*, 315 – 318; c) K. Rotkiewicz, Z. R. Grabowski, A. Krowczynski, W. Kühnle, *J. Lumin.* **1976**, *12/13*, 877 – 885; d) Z. R. Grabowski, K. Rotkiewicz, A. Siemiarczuk, *J. Lumin.* **1979**, *18/19*, 420 – 424.

[12] a) W. Rettig, *Top. Curr. Chem.* **1994**, *169*, 253 – 299; b) W. Rettig, *Angew. Chem.* **1986**, *98*, 969 – 986; *Angew. Chem. Int. Ed. Engl.* **1986**, *25*, 971 – 988.

[13] a) K. A. Zachariasse, T. Vonderhaar, A. Hebecker, U. Leinhos, W. Kühnle, *Pure. Appl. Chem.* **1993**, 65, 1745 – 1750; b) Y. V. Il'ichev, W. Kühnle, K. A. Zachariasse, *J. Phys. Chem.* **1998**, *102*, 5670 – 5680.

[14] A. L. Sobolewski, W. Domcke, *Chem. Phys. Lett.* **1996**, 250, 428 – 436.

[15] M. E. Casida in *Recent Advances in Density Functional Theory* (Ed.: D. P. Chong), World Scientific, Singapore, **1999**, pp. 100 – 110.

[16] E. K. U. Gross, W. Kohn, *Adv. Quantum Chem.* **1990**, *21*, 255 – 291.

[17] M. E. Casida, C. Jamorski, K. C. Casida, D. R. Salahub, *J. Chem. Phys.* **1998**, 108, 4439 – 4449.

[18] C. Adamo, G. E. Scuseria, V. Barone, *J. Chem. Phys.* **1999**, *111*, 2889 – 2899.

[19] E. Lippert, *Z. Naturforsch. A* **1955**, *10*, 541 – 545.

[20] Origin (Version 5.0), Microcal Software, Inc., **1991 – 1997**.

[21] a) Z. R. Grabowski, K. Rotkiewicz, A. Siemiarczuk, D. J. Cowley, W. Baumann, *Nouv. J. Chim.* **1979**, *3*, 443 – 454; b) A. Siemiarczuk, Z. R. Grabowski, A. Krowczynski, M. Asher, M. Ottolenghi, *Chem. Phys. Lett.* **1977**, *51*, 315 – 320.

[22] a) Z. R. Grabowski, J. Dobkowski, *Pure Appl. Chem.* **1983**, *55*, 245 – 252; b) W. Rettig, M. Zander, *Ber. Bunsenges. Phys. Chem.* **1983**, *87*, 1143 – 1149; c) M. Zander, W. Rettig, *Chem. Phys. Lett.* **1984**, *110*, 602 – 610.

[23] a) J. J. La Clair, *J. Am. Chem. Soc.* **1997**, *119*, 7676 – 7684; b) J. J. La Clair, *Angew. Chem.* **1999**, *111*, 3231 – 3233; *Angew. Chem. Int. Ed.* **1999**, *38*, 3045 – 3047.

[24] Gaussian 98 (Revision A.7), M. J. Frisch, G. W. Trucks, H. B. Schlegel, G. E. Scuseria, M. A. Robb, J. R. Cheeseman, V. G. Zakrzewski, J. A. Montgomery, R. E. Stratmann, J. C. Burant, S. Dapprich, J. M. Millam, A. D. Daniels, K. N. Kudin, M. C. Strain, O. Farkas, J. Tomasi, V. Barone, M. Cossi, R. Cammi, B. Mennucci, C. Pomelli, C. Adamo, S. Clifford, J. Ochterski, G. A. Petersson, P. Y. Ayala, Q. Cui, K. Morokuma, D. K. Malick, A. D. Rabuck, K. Raghavachari, J. B. Foresman, J. Cioslowski, J. V. Ortiz, B. B. Stefanov, G. Liu, A. Liashenko, P. Piskorz, I. Komaromi, R. Gomperts, R. L. Martin, D. J. Fox, T. Keith, M. A. Al-Laham, C. Y. Peng, A. Nanayakkara, C. Gonzalez, M. Challacombe, P. M. W. Gill, B. G. Johnson, W. Chen, M. W. Wong, J. L. Andres, M. Head-Gordon, E. S. Replogle, J. A. Pople, Gaussian, Inc., Pittsburgh, PA, **1998**.

[25] A. D. Becke, *J. Chem. Phys.* **1993**, *98*, 5648 – 5652.

[26] C. T. Lee, W. T. Yang, R. G. Parr, *Phys. Rev. B* **1988**, *37*, 785 – 789.

[27] J. S. Binkley, J. A. Pople, W. J. Hehre, *J. Am. Chem. Soc.* **1980**, *102*, 939 – 947.

[28] P. C. Hariharan, J. A. Pople, *Theor. Chim. Acta* **1973**, 28, 213 – 222.

[29] C. H. Choi, M. Kertesz, A. Karpfen, *J. Chem. Phys.* **1997**, *107*, 6712 – 6721.

[30] M. J. S. Dewar, E. G. Zoebisch, E. F. Healy, J. J. P. Stewart, *J. Am. Chem. Soc.* **1985**, *107*, 3902 – 3909.

[31] a) D. J. Tozer, R. D. Amos, N. C. Handy, B. O. Roos, L. Serrano-Andrés, *Mol. Phys.* **1999**, 97, 859 – 868; b) M. E. Casida, F. Gutierrez, J. G. Guan, F. X. Gadea, D. R. Salahub, J. P. Daudey, *J. Chem. Phys.* **2000**, *113*, 7062 – 7071.

[32] C. Jamorski, H. P. Lüthi, J. B. Foresman, unpublished results.

[33] B. Mennucci, A. Toniolo, J. Tomasi, *J. Am. Chem. Soc.* **2000**, *122*, 10 621 – 10 630.

[34] T. H. Reade, S. A. Sim, *J. Chem. Soc.* **1924**, *125*, 157 – 160.

[35] a) H. T. Clarke, H. B. Gillespie, S. Z. Weisshaus, *J. Am. Chem. Soc.* **1933**, *55*, 4571 – 4587; b) M. Gillois, P. Rumpf, *Bull. Soc. Chim. Fr.* **1954**, 112 – 118.

[36] H. Ahlbrecht, E. O. Düber, J. Epsztajn, R. M. K. Marcinkowski, *Tetrahedron* **1984**, *40*, 1157-1165.

[37] S. Kajigaeshi, T. Kakinami, H. Yamasaki, S. Fujisaki, T. Okamoto, *Bull. Chem. Soc. Jpn.* **1988**, *61*, 600 – 602.